Quantifying the effect of difluoromethane on ignition delay times of propane

Eduardo H. Guzman[a], Nora Khalil[b], Rachel A. Schwind[a,c], Richard H. West[b], C. Franklin Goldsmith[a,*]

[a] *Chemical and Environmental Engineering Group, School of Engineering, Brown University, Providence, RI 02912*
[b] *Department of Chemical Engineering, Northeastern University, Boston, MA 02115*
[c] *Institute of Multiscale Thermofluids, School of Engineering, University of Edinburgh, Edinburgh, UK*

Abstract

Poly- and Perfluorinated alkyl substances (PFAS) pose environmental and public health concerns. While incineration remains the most common PFAS remediation method, the complete combustion and pyrolysis mechanism of PFAS is unknown. This study aims to expand our understanding of the kinetics of gas-phase PFAS incineration by measuring the effect of difluoromethane (CH_2F_2) on propane ignition delay times (IDTs). The ignition delay times were measured by OH* emission and end-wall pressure time histories behind the reflected shock wave. Different concentrations of CH_2F_2 were mixed with fuel-lean propane-oxygen mixtures diluted in argon. Experiments were conducted at a nominal reflected shock pressure of P_5 = 1 atm and reflected shock temperatures of $1200 < T_5 < 1800$ K. A new detailed chemical kinetic mechanism is presented. 135 new rate constants were computed using RRKM/ME theory, based upon stationary points computed using ANL0. The new mechanism is in excellent agreement with the measured ignition delay time. A novel sensitivity analysis helps to explain the elementary steps by which CH_2F_2 increases the ignition delay time.

Keywords: CH_2F_2, PFAS, ignition delay time, propane, fluorine

*Corresponding author.

1. Introduction

Difluoromethane (CH_2F_2, R-32) is a valuable compound in the refrigerant industry, serving as a greener alternative to chlorofluorocarbons (CFCs). Unlike CFCs, CH_2F_2 and other hydrofluorocarbons do not deplete the ozone layer and have lower global warming potentials. The increased interest in CH_2F_2 for commercial applications underscored the importance of understanding its thermodynamic and kinetic properties, particularly in the context of flammability and flame suppression. Due to its increased reactivity and flammability, CH_2F_2 presents potential risks to consumer goods and manufacturing processes compared to traditional CFC refrigerant blends. To address this issue, the National Institute of Standards and Technology (NIST) compiled a comprehensive chemical kinetic model for small fluorine-containing refrigerants, including CH_2F_2 [1], and other fluorinated organics [2–4], forming the basis for modeling fluoroorganic reactions in the gas phase.

In addition to the work at NIST, other groups have investigated the impact of small fluorinated species on hydrocarbon combustion, including iodofluorocarbons [5], bromofluorocarbons [6], chlorobromofluorocarbons [7], and hydrofluorocarbons [8]. Depending upon the specifics of (i) the fluorinated species, (ii) the base hydrocarbon, and (iii) the reactor conditions, the dopant either reduced the reactivity, increased the reactivity, or had little-to-no discernible effect.

Ososio et al. conducted flame speed and shock tube experiments for methane, ethane, and propane doped with CF_3Br (Halon-1301) [6]. They observed that CF_3Br accelerated the ignition of CH_4 but decelerated the ignition of C_2H_6 and C_3H_8. Mathieu and coworkers performed similar experiments to quantify the impact of CF_3I (Halon-13001) and CF_2BrCl (Halon-1211) on methane, ethylene, and propane [5, 7]. Consistent with their results for CF_3Br, both CF_3I and CF_2BrCl reduced the ignition delay time of CH_4, increased the ignition delay time of C_2H_4, and had a modest inhibiting effect on C_3H_8. As observed in ref. 8, hydrofluorocarbons tended to enhance the reactivity: C_2HF_5 (HFC-125) and C_3HF_7 (HFC-227) significantly reduced the ignition delay time of methane and had a modest accelerating effect on propane [8]. Most recently, Shaik and coworkers studied the thermal decomposition of CH_2F_2 using laser schlieren densitometry and time-of-flight mass spectrometry in a shock tube [9]. Their analysis provides important quantification of CH_2F_2 decomposition kinetics and subsequent cross reactions on a much shorter timescale.

In addition to their role as potential flame suppressants, the challenges related to the destruction of per- and poly-fluoroalkyl substances (PFAS), prominent environmental contaminants, have led to increased interest in the high-temperature gas-phase kinetics of fluorinated compounds. At present, the most commonly used route for destroying PFAS involves incineration. Unfortunately, the incineration process is poorly understood, and incinerator effluent can contain products of incomplete combustion that are still toxic, *e.g.* small fluoroalkanes like tetrafluoromethane and hexafluoroethane [10]. Computational engineering could help solve the problem of incinerator design, and several groups have sought to quantify many of the unimolecular decomposition pathways [11–20]. These thermal decomposition studies have demonstrated that perfluoroalkanes undergo a complex sequence of dissociation reactions that leads to a mixture of smaller fluorinated compounds [21], including CH_2F_2 and other species that are used as refrigerants or flame retardants.

The present work aims to quantify the impact of difluoromethane on the ignition delay time of propane (C_3H_8) in a shock tube. The ignition delay time (IDT, τ) is a valuable metric for assessing the gas-phase kinetics of polyfluorinated compounds under incinerator-relevant conditions [22]. The experimental ignition delay times are modeled using a newly developed, detailed chemical kinetic mechanism. The mechanism combines a hydrocarbon core mechanism with *ab initio* rate constants and estimates obtained using an automated mechanism generator.

2. Methods

2.1. Experimental Setup and Operation

Experiments were conducted in the Brown Shock Tube (BST) [23] near atmospheric pressures over a temperature range of 1200 – 1800 K. The current configuration of the BST has been modified from previous publications [23–26]. The original diaphragmless driver was replaced with a double diaphragm mechanism. The modifications did not change the dimensions of the driven section (internal diameter of 10 cm and length of 7 m). The new driver has the same internal diameter as the driven section but has a length of 3.3 m. A removable stainless steel insert now isolates the driver and driven section with two layers of the polycarbonate diaphragm (McMaster, 0.020 inches thickness) clamped on either end. The diaphragms were scored in a cross pattern before loading to ensure consistent and repeatable ruptures at the desired loading conditions. The stainless steel insert has a port that connects to a removable hose attached to a 1 L dump tank, roughing pump, and gas line. The double diaphragm interface enables higher loading pressures in the driver section, allowing for higher driver-to-driven pressure ratios. Moreover, the double diaphragm set-up provided increased stability in post-reflected shock pressures relative to prior configurations.

Figure 1 shows the new BST configuration. Shock velocities were calculated using the timing intervals between six piezoelectric pressure transducers (Dynasen, CA-1135) with response times of $\sim$0.1 μs. The Dynasen transducers are spaced 15 cm in series, starting from 90 cm and ending 15 cm upstream of the test window. The shock velocity was interpolated

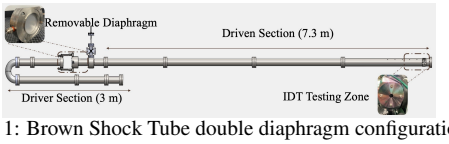

Fig. 1: Brown Shock Tube double diaphragm configuration.

from the final transducer to the test window, resulting in an uncertainty of around 0.2%. The temperature, T_5, and pressure, P_5, behind the reflected shock wave were computed using CANTERA [27] and the SHOCK AND DETONATION TOOLBOX [28] assuming normal shock conditions. The uncertainty of P_5 and T_5 is $\sim$0.5%, based upon prior work with this system.

Table 1: Gas Mixture Composition

CH_2F_2	C_3H_8	O_2	Ar	Dopant ratio	ϕ
—	1.0%	6.0%	93.0%	0.0	0.83
0.1%	1.0%	6.0%	92.9%	0.1	0.85
0.5%	1.0%	6.0%	93.5%	0.5	0.92
2.0%	1.0%	6.0%	91.0%	2.0	1.17
2.0%	0.5%	3.0%	95.5%	4.0	1.50

Mixtures were made manometrically in a 72 L round bottom flask attached to the manifold of the BST. The mixtures were allowed to settle for at least an hour and were agitated with a magnetic stir bar to ensure homogeneity. All compositions contained argon (Airgas, 99.9999%), oxygen (Airgas, 99.9999%), and propane (Airgas, 99.999%) with varying concentrations of CH_2F_2 (Airgas, 99.9%) as seen in Table 1. The concentration of propane and oxygen were held constant, while the addition of CH_2F_2 was offset by a reduction in argon. In Table 1, the "dopant ratio" refers to the proportion of CH_2F_2 relative to C_3H_8, varying from 0.0 to 4.0. All gas combinations were prepared in reference to a 1% propane concentration, except for the final mixture, which was scaled down to 0.5% propane (and thus uses 2% CH_2F_2) to reduce the proportion of reactant gases to bath gas in the driven mixture. These adjustments align with our experimental assumptions, which require dilute conditions for the normal shock equations to remain valid. During complete combustion, the fluorine atoms are assumed to form hydrogen fluoride. The stoichiometric equation used to define the equivalence ratio, ϕ, is given by:

$$a\ CH_2F_2 + b\ C_3H_8 + (a+5b)\ O_2 \rightarrow (a+3b)\ CO_2 + 4b\ H_2O + 2a\ HF \quad (1)$$

Rather than focus on a fixed equivalence ratio, we maintained a constant O_2:C_3H_8 of 6.0. The resulting compositions range from fuel lean at low dopant levels to fuel rich at high dopant levels. This range of equivalence ratios highlights the sensitivity to different submechanisms in the mechanism validation process. More specifically, since our goal is to improve model predictions for small fluorinated compounds, the fuel-rich experiments at high dopant levels will be more sensitive to the kinetics of CH_2F_2 and its various products. The experimental equivalence ratios are provided in Table 1.

The ignition delay times were measured behind the reflected shock using pressure histories and OH* chemiluminescence. The pressure history was measured at the end wall using a PCB transducer (113B21) with a rise time of 1 μs. OH* emission was measured with a photo-multiplier tube (PMT) supplied by Hamamatsu (R928) at the side wall. The PMT was attached to a lens tube (Thorlabs, 6.43 cm length, $\varnothing$2.54 cm) set with a narrow-bandpass filter (Edmund Optics, 313 nm center wavelength, FWHM 10.00 ± 2.0 nm) and a semi-planar convex lens (Thorlabs, $\varnothing$2.54 cm). The filter and the lens were placed at their focal lengths away from the aperture of the PMT, 5 mm and 20 mm, respectively. The OH* emission detector was then aligned perpendicular to the length of the shock tube at the side wall. The distance from the aperture of the PMT to the test windows was roughly 6.60 cm.

The ignition delay times were defined by extrapolating the maximum gradient of the relative OH* emission signal to the baseline. The gradient was calculated using a second-order centered difference approximation [29]. The error of this calculation scales with $\Delta t^2 \sim 10^{-5}$ ms. The pressure histories on the end wall were processed similarly to OH* IDTs and then compared. IDTs with a differential greater than 1% from both methods were disregarded. Example pressure and OH* emission profiles can be seen in Figure 2.

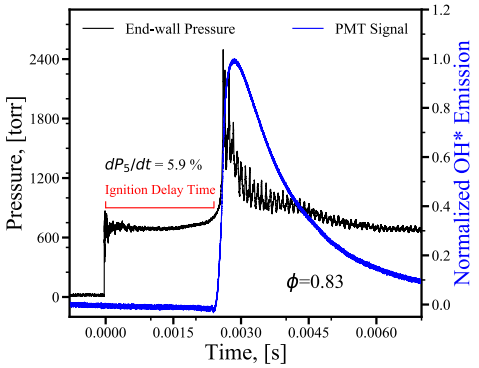

Fig. 2: Pressure and OH* emission profiles of propane (C_3H_8:1/O_2:6/Ar:93) at 1356 K.

2.2. Computational Methodology and Mechanism Development

The elementary kinetic mechanism combines two pre-existing mechanisms from the literature with newly developed rate coefficients. The hydrocarbon core was taken from Ref. 29, based on the small-molecule chemistry developed at Argonne National Laboratory, which we refer to as the "ANL" mecha-

nism [30]. As discussed below, additional hydrocarbon mechanisms were considered. The ANL mechanism was combined with the mechanism taken from Ref. 31, which consists of H- and F-abstraction reactions involving fluorinated compounds. The resulting combined mechanism served as an initial starting point; the present work builds off this initial mechanism to include the unimolecular decomposition of several C_1 and C_2 species. For comparison purposes, the recent CH_2F_2 mechanism from NIST was additionally tested [4].

REACTION MECHANISM GENERATOR (RMG) software [32–35] was used to propose new reactions for addition into the initial mechanism. The reaction system was simulated in RMG using a range-based `simpleReactor()` from 1000–1800 K and 1–10 bar with pressure-dependent chemistry included. Proposed reactions were then refined using computational kinetics methods described below. Updated reactions were then added to the initial mechanism, and ignition delays were re-simulated. This process was repeated until no new reactions were required to simulate the experimental ignition delay times with sufficient accuracy.

All electronic structure calculations were done using the ANL0 compound method [36]. When appropriate, torsional scans were performed in 10° increments using M06-2X/cc-pVTZ [37], and the resulting potential was used to compute the partition function for hindered internal rotation via summation over the energy levels for the corresponding 1-D Schrödinger equation. All density functional theory calculations were performed using GAUSSIAN09 [38]. All wavefunction methods were performed using MOLPRO [39].

All RRKM/ME calculations were performed using MESS, which is part of the PAPR family of computational kinetics software [40, 41]. All elementary reactions with a first-order saddle point were treated using fixed transition state theory, according to which the transition state is assumed to be the saddle point, and the corresponding partition function is assumed to be a harmonic oscillator. For the barrierless reactions, variational analysis was performed using the semi-empirical `PhaseSpaceTheory` method in MESS [42–44]. The coefficient of the interaction potential, αr^{-6}, was set so that the high-pressure limit for the rate coefficient of the radical-radical recombination was approximately 3×10^{-11} cm^3/molecule-s. In cases with a clear analogy to hydrocarbon chemistry, α was adjusted to match (but not exceed) the high-pressure limit of the hydrocarbon case. For example, for the recombination of difluoromethyl radical, $CHF_2 + CHF_2 \rightarrow CHF_2CHF_2$, α was adjusted so that the high-pressure limit constant was $k^{\infty}(800\text{ K}) = 1.2 \times 10^{-11}$ cm^3/molecule-s and $k^{\infty}(1800\text{K}) = 1.3 \times 10^{-11}$ cm^3/molecule-s, based upon the corresponding high-pressure limit values for $CH_3 + CH_3 \rightarrow C_2H_6$ of $k^{\infty}(800\text{K}) = 3.9 \times 10^{-11}$ cm^3/molecule-s and $k^{\infty}(1800\text{K}) = 2.0 \times 10^{-11}$ cm^3/molecule-s. Future work will replace this form of variational transition state theory with a more rigorous variable reaction coordinate transition state theory. Collisional energy transfer was assumed to follow a simple single exponential model, with $\langle \Delta E_{\text{down}} \rangle$ = 100 $(T/298[\text{K}])^{0.85}$ cm^{-1} for C_1 species and $\langle \Delta E_{\text{down}} \rangle$ = 200 $(T/298[\text{K}])^{0.85}$ cm^{-1} for C_2 species. The thermophysical properties for all fluorinated species were taken from Ref. 31.

2.3. Simulations and Sensitivity Analysis

CANTERA was used to compute ignition delay times in a homogenous, adiabatic, constant-volume zero-dimensional `Reactor()`. Ignition delays were calculated to match the experimental conditions at 1±0.015 atm, with temperatures of 1282–1887 K, and initial mole fractions as described in Table 1. The calculation of the modeled IDTs closely mirrored the experimental approach, except for the use of the simulated OH species histories.

Sensitivity analyses were performed to determine which reactions had considerable influence on the simulated ignition delay times. The reference IDTs (τ_{ref}) were calculated without any modification to the newly developed mechanism. To quantify the impact of the i^{th} reaction on the IDTs, the corresponding rate constant, k_i, was increased by 1%. The IDTs were then recalculated with this single rate constant perturbation, τ_i. The resulting normalized sensitivity coefficient, S_i, was computed for each reaction:

$$S_i = \frac{\partial \ln \tau}{\partial \ln k_i} = \frac{k_{i,\text{ref}}}{\tau_{\text{ref}}} \left(\frac{\tau_i - \tau_{\text{ref}}}{k_i - k_{i,\text{ref}}} \right). \quad (2)$$

Sensitivities were calculated at a representative low, middle, and high temperature (1292, 1467, and 1818 K, respectively). The sensitivity coefficients, as defined by Eq. (2), highlight a large number of hydrocarbon reactions that have little to do with fluorine chemistry, many of which are well characterized (*e.g.* $H + O_2 \rightleftharpoons O + OH$). While undoubtedly critical for ignition, these reactions do not help us understand the fire-suppressing behavior of CH_2F_2. Instead, we wish to isolate the reactions most responsible for the increase in observed τ as the amount of CH_2F_2 in the mixture increases. To do so, we define a new sensitivity coefficient, S_i^{sup}, which takes the ratio of ignition delay time with the highest dopant ratio, $\tau^{4.0}$, to the ignition delay time with the lowest non-zero dopant ratio, $\tau^{0.1}$, and then see how minor perturbations in the rate constants affect this ratio:

$$S_i^{\text{sup}} = \frac{k_{i,\text{ref}}}{\tau_{\text{ref}}^{4.0}/\tau_{\text{ref}}^{0.1}} \left(\frac{\tau_i^{4.0}/\tau_i^{0.1} - \tau_{\text{ref}}^{4.0}/\tau_{\text{ref}}^{0.1}}{k_i - k_{i,\text{ref}}} \right). \quad (3)$$

These suppression-focused sensitivity coefficients identified which reactions were important in increasing the ignition delay time when the amount of CH_2F_2 was increased. This approach was critical in the iterative mechanism construction since it allowed us to

determine which of the fluorochemical reactions that RMG proposed were important.

3. Results and Discussion

3.1. Ignition Delay Times

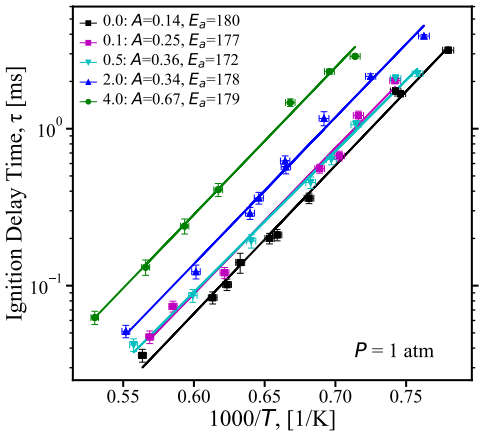

Fig. 3: Measured ignition delay (symbols) of propane with dopant ratio CH_2F_2:C_3H_8 of 0.0 (black), 0.1 CH_2F_2 (magenta), 0.5 CH_2F_2 (cyan), 2.0 CH_2F_2 (blue), and 4.0 CH_2F_2 (green) in excess argon at 1 atm. The lines are the corresponding regression to the data, in the format $\tau = A\exp[E_a/RT]$, with A in ms and E_a in kJ/mol.

The measured ignition delay times for the different dopant ratios are presented in Figure 3. As anticipated, the addition of CH_2F_2 increases the ignition delay. To a reasonable approximation, the ignition delay time increased linearly with increasing dopant ratio (see Supplemental Materials for details).

A one-sample t-test using the R software was performed on the slopes and y-intercept of the linear regressions from the doped cases, which were tested on the slope and y-intercept of the linear regression of the neat case [45]. The slopes of the regressions were significantly similar (p-value > 0.05, $|t| = 2.04$), while the y-intercepts of the regression were significantly different (p-value < 0.05, $|t| = 5.13$). As seen in Figure 3, the regression slope (E_a in the figure) is consistent in all five cases, with less than 3% deviation from the mean of $E_a = 177$ kJ/mol. The intercept, in contrast, increases approximately linearly with increasing dopant ratio. For the two lowest non-zero dopant ratios, 0.1 (magenta squares) and 0.5 (cyan triangles), the measured ignition delays were virtually identical.

3.2. Mechanism Validation

The first step in the analysis was to focus on the ignition delay time of undoped propane, with nominal pressures of 1 atm and excess oxygen. Five different mechanisms were selected from the literature: ANL [29], San Diego [46], CRECK [47], AramcoMech 3.0 [48], and NUIGMech 1.3 [49].

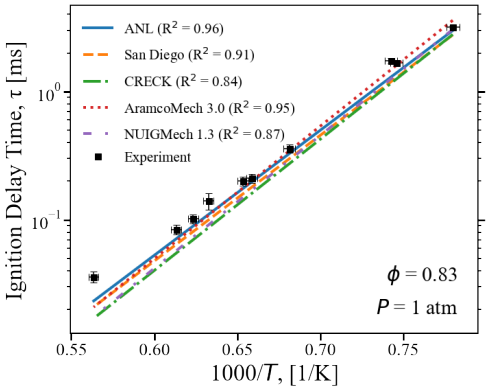

Fig. 4: Measured ignition delay of propane (symbols) compared to ANL [29], San Diego [46], CRECK [47], AramcoMech3.0 [48], and NUIGMech 1.3 [49] mechanisms.

The simulated IDT is plotted with the measured IDT in Figure 4, together with the corresponding coefficient of determination, R^2 (in $\ln\tau$). All five mechanisms perform well. The agreement between all five models and the data confirms that the new BST diagnostic works as intended. Based on these results, the ANL mechanism was selected as the base hydrocarbon mechanism. Similar results were obtained when the NUIGMech was used instead (the most recently validated propane mechanism); these results are included in the Supplemental Material.

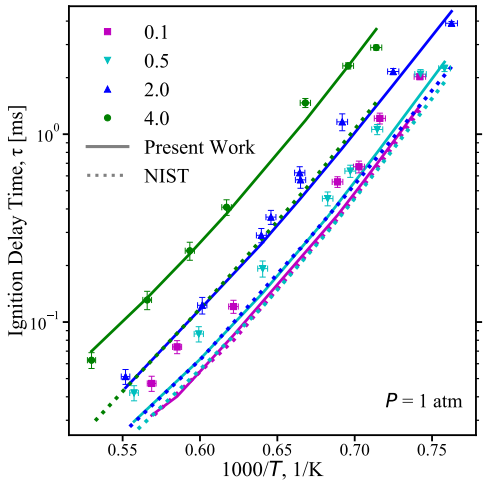

Fig. 5: Measured ignition delay (symbols) compared to present work (solid line) and NIST mechanism (dotted line with ANL as the base hydrocarbon mechanism [4, 29].

The CH_2F_2 mechanism by Burgess and coworkers [4] at NIST originally used GRI-Mech for the hydrocarbon chemistry subset. To facilitate use in propane autoignition, we replaced that portion of the mechanism with the ANL mechanism from Ref. [29]. Although the NIST mechanism predicts trends correctly, it fails to predict the ignition delay times quan-

titatively, particularly for the higher dopant concentrations (see dotted lines in Figure 5).

Figure 5 presents the new mechanism, based upon the iterative refinement process in which RMG would propose a missing reaction, and then transition state theory was used to update the results. As part of this procedure, RMG highlighted the importance of the difluoromethyl radical, CHF_2. Of particular importance were various recombination reactions involving CHF_2 and other radicals (both fluorinated and organic) that were present before ignition. This process led to a cascade of new reactions to consider. Ultimately, radical-radical, unimolecular decomposition, and phenomenological (well-skipping) reactions were added for the following potential energy surfaces: CH_2F, CHF_2, CH_3F, CH_2F_2, FCO, CHFO, CHF_2O, CHF_2OH, CF(O)OH, CHF_2O_2, CHF_2OOH, CH_3CHF_2, CH_2FCHF_2, and CHF_2CHF_2. Additionally, RMG suggested two new H-abstraction reactions, $CH_2CH + CH_2F_2$ and $H + CHF_2CHF_2$, which were important for the ignition delay but were not considered in Ref. 31. In total, the iterative procedure resulted in 135 new rate constants that were added to the 85 abstraction reactions in our prior work. Consistent with our mechanism, the analysis by Shaik et al. found that HF elimination was the only unimolecular decomposition channel for CH_2F_2 [9].

As can be seen in Figure 5, the new mechanism is in excellent agreement with the experimental data for all five dopant ratios.

3.3. Sensitivity Analyses

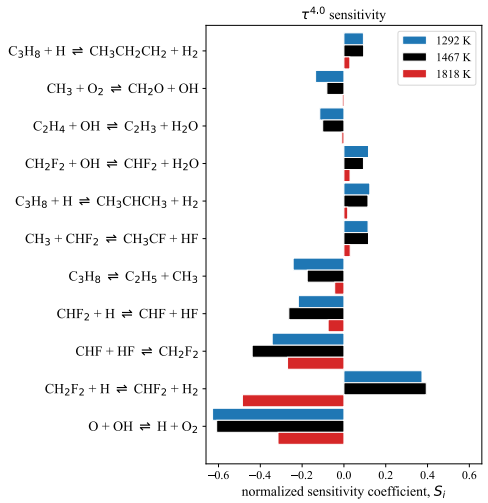

Fig. 6: Normalized sensitivity coefficients for the mixture with a dopant ratio of 4.0 at three temperatures.

Figure 6 summarizes the normalized sensitivity coefficients for the mixture with dopant ratio of 4. The 11 reactions that had the highest average sensitivity coefficient for all three temperatures are presented. As expected, the reaction $O + OH \rightleftharpoons H + O_2$ is among the most sensitive, but the importance of this reaction is otherwise omitted from the discussion below. Whereas the sensitivity coefficients for the low (1292 K) and intermediate (1467 K) temperatures are fairly consistent, the sensitivity coefficients for the high-temperature case (1818 K) are different. The ignition delay time at the highest temperatures is highly sensitive to only a few reactions, with the two most sensitive reactions being the decomposition of CH_2F_2 and H-abstraction from CH_2F_2 via H atom.

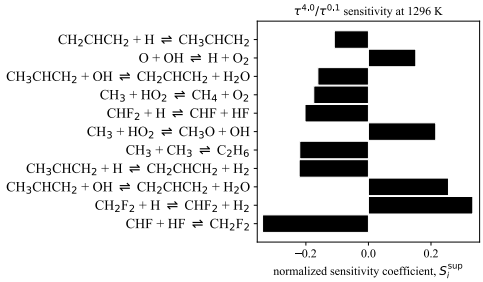

Fig. 7: Normalized sensitivity coefficients for the suppression-focused sensitivity analysis, Eq. (3).

Figure 7 presents the suppression-focused sensitivity coefficients, Eq. (3), at 1296 K. According to this new metric, some reactions will decrease the spread between $\tau^{4.0}$ and $\tau^{0.1}$ (*i.e.*, $S_i^{\text{sup}} < 0$), whereas other reactions will increase the spread between $\tau^{4.0}$ and $\tau^{0.1}$ (*i.e.*, $S_i^{\text{sup}} > 0$). As seen in the figure, the two most important reactions involve CH_2F_2, but they have opposite signs.

The reaction $CH_2F_2 + H \rightleftharpoons CHF_2 + H_2$ has a large positive S_i^{sup}, because it consumes H atoms, thereby decreasing the rate of important chain branching reactions, such as $H + O_2 \rightarrow O + OH$. The larger the concentration of CH_2F_2, the more effective it is at scavenging H atoms. In contrast, HF elimination from CH_2F_2 has a large negative S_i^{sup} because it removes CH_2F_2 as an H scavenger and replaces it with a more reactive singlet carbene, CHF.

Under the experimental conditions, the well-skipping reaction $CHF_2 + H \rightleftharpoons CHF + HF$ runs in the reverse direction; increasing the rate constant increases the rate at which H atoms are regenerated, and thus it decreases both $\tau^{4.0}$ and $\tau^{0.1}$. It has a negative S_i^{sup} because it decreases $\tau^{4.0}$ more than it decreases $\tau^{0.1}$. The reactions of H and OH with propene, CH_3CHCH_2, also have negative suppression-focused sensitivity coefficients but for a different reason. These reactions shift the composition of the radical pool from the more reactive H and OH to the less reactive allyl, CH_2CHCH_2, and increasing those rate constants increases τ across the board. This effect is more pronounced for the 0.1 dopant ratio mixture than for the 4.0 dopant ratio mixture, and thus increasing those rate constants increases $\tau^{0.1}$ more than it increases $\tau^{4.0}$.

One immediate distinction between the present

work and the collective work of Peterson and coworkers is that our ratio of "dopant" to hydrocarbon is significantly greater than in refs. 5–8. The comparative abundance of fluorinated species in the present work has a strong impact on the observed sensitivities. With this caveat in mind, if we contrast CH_2F_2 with other fluorinated compounds, we begin to form a more complete picture of the small-molecule chemistry. First, much of the decrease in reactivity observed with CF_3Br and CF_3I is due to the formation of CF_3 as a decomposition product [5]. Although CF_3 can participate in many reactions, some of which could increase reactivity, the net effect of CF_3 is to act like a radical scavenger. Similarly, for CF_2BrCl, much of the inhibitory effect comes from the liberated Br, which also acts as a radical scavenger – either directly (*e.g.* $C_2H_3 + Br$) or indirectly (*e.g.* $HBr + H$). Other contributions from CF_2BrCl to the total reactivity come from CF_2 as a reactive intermediate. Collectively, these results were more pronounced for methane than for propane.

The pyrolysis and combustion of CH_2F_2, in contrast, does not lead to significant amounts of CF_3. The main route for CF_3 production from CH_2F_2 is an indirect route via CHF_2, but it is comparatively minor under the current conditions. Similarly, the net rate of CF_2 production is quite small. In their investigation into the impact of hydrofluorocarbons on alkane ignition, Osorio et al. found that neither C_2HF_5 nor C_3HF_7 had a substantial impact on the ignition delay time of C_3H_8, but that the reaction $CHF_2 + OH \rightleftharpoons CHFO + HF$ was the most significant reaction in terms of the inhibition of the C_3H_8 ignition delay time [8]. Although our mechanism includes this well-skipping reaction, it is not among the most sensitive for our conditions, perhaps because the overall yield of CHF_2 is low in our system.

Collectively, the present work complements the experimental and modeling studies of refs. 5–9 regarding our understanding of small-molecule kinetics for fluorine-hydrocarbon combustion. Future work will expand the current mechanism to include their validation targets.

4. Conclusions

The ignition delay times of different mixtures of CH_2F_2, C_3H_8, and O_2 in Ar were measured in a shock tube via OH* chemiluminescence. Experiments were conducted at a reflected shock pressure of P_5 = 1 atm and reflected shock temperatures of $1200 < T_5 < 1700$ K. Increasing the CH_2F_2:C_3H_8 ratio while holding the O_2:C_3H_8 ratio constant reduced the reactivity of the system, thereby increasing the ignition delay time. A new detailed chemical kinetic mechanism for $CH_2F_2/C_3H_8/O_2$ blends was developed using an iterative procedure. The automatic mechanism generator RMG was used to propose reactions involving fluorinated species, and these reactions were subsequently refined using high-level computational methods. The new mechanism is in excellent agreement with the measured data. CH_2F_2 increases the ignition delay time because it acts as a scavenger of H atoms, thereby decreasing the net rate of the most important chain branching reaction in high-temperature autoignition.

Declaration of competing interest

The authors declare that they have no known competing financial interests or personal relationships that could have appeared to influence the work reported in this paper.

Acknowledgments

The authors are grateful to Dr. Robert Tranter and Dr. Raghu Sivaramakrishnan for numerous helpful discussions on difluoromethane and in the development of the CH_2F_2 mechanism. This work was supported by the U.S. Army Corps of Engineers, Strategic Environmental Research and Development Program (SERDP), through award number 008305, with Dr. Andrea Leeson as the program manager. RAS gratefully acknowledges support from the Office of Naval Research (N00014-20-1-2713), with Dr. Maria Mederios as the program manager. CFG gratefully acknowledges additional support from the US Department of Energy, Basic Energy Science, through grant number DE-SC0019489, with Dr. Wade Sisk as the program manager. This material is based upon work also supported by the National Science Foundation under Grant No. 1751720 and by the National Science Foundation Graduate Research Fellowship (for NK) under Grant No. 1938052.

*franklin_goldsmith@brown.edu

Supplementary material

The Supplemental Material includes:

- Experimental data for ignition delay time measurements of $CH_2F_2/C_3H_8/O_2$/Ar mixtures simulated with NUIGMech 1.3 and new mechanism [49].
- Normalized sensitivity coefficients for dopant ratios of 0.0 and 4.0 at 1292, 1467, and 1818 K.
- Suppression-focused sensitivity analysis results at 1292, 1467, and 1818 K.
- chemical kinetic mechanism (in `yaml` format)

References

[1] V. I. Babushok, D. R. J. Burgess, D. K. Kim, M. J. Hegetschweiler, G. T. Linteris, Modeling of combustion of fluorine-containing refrigerants, Tech. rep., National Institute of Standards and Technology (U.S.) (Nov. 2021). doi:10.6028/nist.tn.2170.

[2] I. H. Bell, P. A. Domanski, M. O. McLinden, G. T. Linteris, The hunt for nonflammable refrigerant blends to replace R-134a, International Journal of Refrigeration 104 (2019) 484–495. doi:10.1016/j.ijrefrig.2019.05.035.

[3] D. R. Burgess, J. A. Manion, Rate Constants for Abstraction of H from the Fluoromethanes by H, O, F, and OH, Journal of Physical and Chemical Reference Data 50 (2) (2021). doi:10.1063/5.0028874.

[4] D. R. Burgess Jr., V. I. Babushok, J. A. Manion, A chemical kinetic mechanism for combustion and flame propagation of $CH_2F_2/O_2/N_2$ mixtures, International Journal of Chemical Kinetics 54 (3) (2022) 154–187. doi:https://doi.org/10.1002/kin.21549.

[5] O. Mathieu, J. Goulier, F. Gourmel, M. Mannan, N. Chaumeix, E. Petersen, Experimental study of the effect of CF_3I addition on the ignition delay time and laminar flame speed of methane, ethylene, and propane, Proceedings of the Combustion Institute 35 (2015) 2731–2739. doi:10.1016/j.proci.2014.05.096.

[6] C. H. Osorio, A. J. Vissotski, E. L. Petersen, M. S. Mannan, Effect of CF_3Br on C1–C3 ignition and laminar flame speed: Numerical and experimental evaluation, Combustion and Flame 160 (2013) 1044–1059. doi:10.1016/j.combustflame.2013.01.025.

[7] O. Mathieu, C. Keesee, C. Gregoire, E. L. Petersen, Experimental and Chemical Kinetics Study of the Effects of Halon 1211 (CF_2BrCl) on the Laminar Flame Speed and Ignition of Light Hydrocarbons, The Journal of Physical Chemistry A 119 (2015) 7611–7626. doi:10.1021/acs.jpca.5b00959.

[8] C. Osorio, A. Morones, J. Hargis, E. Petersen, M. Mannan, Effect of C_2HF_5 and C_3HF_7 on methane and propane ignition and laminar flame speed: Experimental and numerical evaluation, Journal of Loss Prevention in the Process Industries 48 (2017) 21–31. doi:10.1016/j.jlp.2017.04.003.

[9] R. A. Shaik, A. W. Jasper, P. T. Lynch, R. SIVARAMAKRISHNAN, R. S. Tranter, Initiation and carbene induced radical chain reactions in ch_2f_2 pyrolysis, ChemPhysChem (5 2024). doi:10.1002/cphc.202400362.

[10] T. Yamada, P. H. Taylor, R. C. Buck, M. A. Kaiser, R. J. Giraud, Thermal degradation of fluorotelomer treated articles and related materials, Chemosphere 61 (2005) 974–984. doi:10.1016/j.chemosphere.2005.03.025.

[11] M. Khan, S. So, G. da Silva, Decomposition kinetics of perfluorinated sulfonic acids, Chemosphere 238 (2020) 124615. doi:https://doi.org/10.1016/j.chemosphere.2019.124615.

[12] D. S. Farina, S. K. Sirumalla, E. J. Mazeau, R. H. West, Extensive high-accuracy thermochemistry and group additivity values for halocarbon combustion modeling, Industrial & Engineering Chemistry Research 60 (43) (2021) 15492–15501. doi:10.1021/acs.iecr.1c03076.

[13] M. Altarawneh, M. H. Almatarneh, B. Z. Dlugogorski, Thermal decomposition of perfluorinated carboxylic acids: Kinetic model and theoretical requirements for PFAS incineration, Chemosphere 286 (2022) 131685. doi:https://doi.org/10.1016/j.chemosphere.2021.131685.

[14] M. Y. Khan, J. Song, M. Narimani, G. da Silva, Thermal decomposition mechanism and kinetics of perfluorooctanoic acid (PFOA) and other perfluorinated carboxylic acids: a theoretical study, Environ. Sci.: Processes Impacts 24 (2022) 2475–2487. doi:10.1039/D2EM00259K.

[15] M. A. Adi, M. Altarawneh, Thermal decomposition of heptafluoropropylene-oxide-dimer acid (GenX), Chemosphere 289 (2022) 133118. doi:https://doi.org/10.1016/j.chemosphere.2021.133118.

[16] C.-B. Paultre, A. M. Mebel, K. E. O'Shea, Computational study of the gas-phase thermal degradation of perfluoroalkyl carboxylic acids, The Journal of Physical Chemistry A 126 (46) (2022) 8753–8760. doi:10.1021/acs.jpca.2c06437.

[17] X. Ding, X. Song, X. Chen, D. Ding, C. Xu, H. Chen, Degradation and mechanism of hexafluoropropylene oxide dimer acid by thermally activated persulfate in aqueous solutions, Chemosphere 286 (2022) 131720. doi:https://doi.org/10.1016/j.chemosphere.2021.131720.

[18] N. H. Weber, L. J. Dixon, S. P. Stockenhuber, C. C. Grimison, J. A. Lucas, J. C. Mackie, M. Stockenhuber, E. M. Kennedy, Thermal decomposition of PFOA: Influence of reactor and reaction conditions on product formation, Chemical Engineering Science 278 (2023) 118924. doi:https://doi.org/10.1016/j.ces.2023.118924.

[19] A. Alinezhad, H. Shao, K. Litvanova, R. Sun, A. Kubatova, W. Zhang, Y. Li, F. Xiao, Mechanistic investigations of thermal decomposition of perfluoroalkyl ether carboxylic acids and short-chain perfluoroalkyl carboxylic acids, Environmental Science & Technology 57 (23) (2023) 8796–8807. doi:10.1021/acs.est.3c00294.

[20] J. Blotevogel, R. J. Giraud, A. K. Rappé, Incinerability of PFOA and HFPO-DA: Mechanisms, kinetics, and thermal stability ranking, Chemical Engineering Journal 457 (2023) 141235. doi:https://doi.org/10.1016/j.cej.2022.141235.

[21] F. Xiao, P. C. Sasi, B. Yao, A. Kubátová, S. A. Golovko, M. Y. Golovko, D. Soli, Thermal stability and decomposition of perfluoroalkyl substances on spent granular activated carbon, Environmental Science & Technology Letters 7 (2020) 343–350. doi:10.1021/acs.estlett.0c00114.

[22] O. Mathieu, P. Diévart, M. Turner, D. Mohr, C. Grégoire, S. Alturaifi, L. Catoire, E. Petersen, Experimental and detailed kinetics modeling study of the fire suppressant properties of di(2,2,2trifluoroethyl) carbonate, Proceedings of the Combustion Institute 39 (1) (2023) 499–510. doi:https://doi.org/10.1016/j.proci.2022.07.078.

[23] M. E. Fuller, M. Skowron, R. S. Tranter, C. F. Goldsmith, A modular, multi-diagnostic, automated shock tube for gas-phase chemistry, Review of Scientific Instruments 90 (2019) 064104. doi:10.1063/1.5095077.

[24] C. A. Almodovar, C. F. Goldsmith, Laser schlieren study of the thermal decomposition of 2-ethylhexylnitrate, Proceedings of the Combustion Institute 38 (2021) 997–1005. doi:10.1016/j.proci.2020.07.105.

[25] M. Döntgen, M. E. Fuller, S. Peukert, D. Nativel, C. Schulz, K. A. Heufer, C. F. Goldsmith, Shock tube study of the pyrolysis kinetics of di- and trimethoxy methane, Combustion and Flame 242 (8 2022). doi:10.1016/j.combustflame.2022.112186.

[26] M. E. Fuller, C. F. Goldsmith, Shock tube laser schlieren study of the pyrolysis of isopropyl nitrate, Journal of Physical Chemistry A 123 (2019) 5866–5876. doi:10.1021/acs.jpca.9b03325.

[27] D. G. Goodwin, R. L. Speth, H. K. Moffat, B. W. Weber, Cantera: An object-oriented software toolkit for chemical kinetics, thermodynamics, and transport processes, version 2.6.0 (2023). doi:10.5281/zenodo.4527812.

[28] S. T. Browne, J. L. Ziegler, N. P. Bitter, B. E. Schmidt, J. Lawson, J. E. G. Shepherd, SDToolbox: Numerical Solution Methods for Shock and Detonation Jump Conditions, version 3 (2018).

[29] M. E. Fuller, A. Mousse-Rayaleh, N. Chaumeix, C. F. Goldsmith, Laminar flame speeds and ignition delay times for isopropyl nitrate and propane blends, Combustion and Flame 242 (2022) 112187. doi:https://doi.org/10.1016/j.combustflame.2022.112187.

[30] J. A. Miller, R. Sivaramakrishnan, Y. Tao, C. F. Goldsmith, M. P. Burke, A. W. Jasper, N. Hansen, N. J. Labbe, P. Glarborg, J. Zádor, Combustion chemistry in the twenty-first century developing theory-informed chemical kinetics models, Progress in Energy and Combustion Science 83 (2021) 100886. doi:https://doi.org/10.1016/j.pecs.2020.100886.

[31] S. Sharma, K. Abeywardane, C. F. Goldsmith, Theory-Based Mechanism for Fluoromethane Combustion I: Thermochemistry and Abstraction Reactions, Journal of Physical Chemistry A 127 (6) (2023) 1499–1511. doi:10.1021/acs.jpca.2c06623.

[32] W. H. Green, R. H. West, Rmg - reaction mechanism generator version 3.1.0 (2021).

[33] C. W. Gao, J. W. Allen, W. H. Green, R. H. West, Reaction Mechanism Generator: Automatic construction of chemical kinetic mechanisms, Comput. Phys. Commun. 203 (2016) 212–225. doi:10.1016/j.cpc.2016.02.013.

[34] M. Liu, A. Grinberg Dana, M. S. Johnson, M. J. Goldman, A. Jocher, A. M. Payne, C. A. Grambow, K. Han, N. W. Yee, E. J. Mazeau, K. Blondal, R. H. West, C. F. Goldsmith, W. H. Green, Reaction Mechanism Generator v3.0: Advances in Automatic Mechanism Generation, J. Chem. Inf. Model. 61 (6) (2021) 2686–2696. doi:10.1021/acs.jcim.0c01480.

[35] M. Johnson, X. Dong, A. Grinberg Dana, Y. Chung, D. Farina Jr, R. Gillis, M. Liu, N. Yee, K. Blondal, E. Mazeau, C. Grambow, A. Payne, K. Spiekermann, H.-W. Pang, C. F. Goldsmith, R. West, W. Green, The RMG Database for Chemical Property Prediction, J. Chem. Inf. Model. (in press) (2022).

[36] S. J. Klippenstein, L. B. Harding, B. Ruscic, Ab initio computations and active thermochemical tables hand in hand: Heats of formation of core combustion species, The Journal of Physical Chemistry A 121 (2017) 6580–6602.

[37] Y. Zhao, D. Truhlar, The M06 suite of density functionals for main group thermochemistry, thermochemical kinetics, noncovalent interactions, excited states, and transition elements: two new functionals and systematic testing of four M06-class functionals and 12 other functionals, Theoretical Chemistry Accounts 120 (2008) 215—241.

[38] M. J. Frisch, G. W. Trucks, H. B. Schlegel, G. E. Scuseria, M. A. Robb, J. R. Cheeseman, G. Scalmani, V. Barone, G. A. Petersson, H. Nakatsuji, X. Li, M. Caricato, A. V. Marenich, J. Bloino, B. G. Janesko, R. Gomperts, B. Mennucci, H. P. Hratchian, J. V. Ortiz, A. F. Izmaylov, J. L. Sonnenberg, D. Williams-Young, F. Ding, F. Lipparini, F. Egidi, J. Goings, B. Peng, A. Petrone, T. Henderson, D. Ranasinghe, V. G. Zakrzewski, J. Gao, N. Rega, G. Zheng, W. Liang, M. Hada, M. Ehara, K. Toyota, R. Fukuda, J. Hasegawa, M. Ishida, T. Nakajima, Y. Honda, O. Kitao, H. Nakai, T. Vreven, K. Throssell, J. A. Montgomery, Jr., J. E. Peralta, F. Ogliaro, M. J. Bearpark, J. J. Heyd, E. N. Brothers, K. N. Kudin, V. N. Staroverov, T. A. Keith, R. Kobayashi, J. Normand, K. Raghavachari, A. P. Rendell, J. C. Burant, S. S. Iyengar, J. Tomasi, M. Cossi, J. M. Millam, M. Klene, C. Adamo, R. Cammi, J. W. Ochterski, R. L. Martin, K. Morokuma, O. Farkas, J. B. Foresman, D. J. Fox, Gaussian 09 Revision D.01, Gaussian Inc. Wallingford CT (2013).

[39] H.-J. Werner, P. J. Knowles, G. Gia, F. R. Manby, M. Schütz, P. Celani, W. Györffy, D. Kats, T. Korona, R. Lindh, A. Mitrushenkov, G. Rauhut, K. R. Shamasundar, T. B. Adler, R. D. Amos, A. Bernhardsson, A. Berning, D. L. Cooper, M. J. O. Deegan, A. J. Dobbyn, F. Eckert, E. Goll, C. Hampel, A. Hesselmann, G. Hetzer, T. Hrenar, G. Jansen, C. Köppl, Y. Liu, A. W. Lloyd, R. A. Mata, A. J. May, S. J. McNicholas, W. Meyer, M. E. Mura, A. Nicklass, D. P. O'Neill, P. Palmieri, D. Peng, K. Pflüger, R. Pitzer, M. Reiher, T. Shiozaki, H. Stoll, A. J. Stone, R. Tarroni, T. Thorsteinsson, M. Wang, Molpro, version 2015.1, a package of ab initio programs (2015).

[40] Y. Georgievskii, S. J. Klippenstein, MESS: Master equation system solver 2016.3.23 (2016).

[41] Y. Georgievskii, J. A. Miller, M. P. Burke, S. J. Klippenstein, Reformulation and solution of the master equation for multiple-well chemical reactions, The Journal of Physical Chemistry A 117 (2013) 12146–12154. doi:10.1021/jp4060704.

[42] J. O. Hirschfelder, E. Wigner, Some quantum-mechanical considerations in the theory of reactions involving an activation energy, The Journal of Chemical Physics 7 (1939) 616.

[43] W. H. Miller, Unified statistical model for "complex" and "direct" reaction mechanisms, The Journal of Chemical Physics 65 (1976) 2216–2223.

[44] W. J. Chesnavich, L. Bass, T. Su, M. T. Bowers, Multiple transition states in unimolecular reactions: A transition state switching model. application to the $C_4H_8^+\cdot$ system, The Journal of Chemical Physics 74 (1981) 2228–2246.

[45] R Core Team, R: A language and environment for statistical computing, version 4.3.2 (2021).

[46] U. of California at San Diego Mechanical, A. E. C. Research), Chemical-kinetic mechanisms for combustion applications, http://combustion.ucsd.edu (2012).

[47] G. Bagheri, E. Ranzi, M. Pelucchi, A. Parente, A. Frassoldati, T. Faravelli, Comprehensive kinetic study of combustion technologies for low environmental impact: Mild and oxy-fuel combustion of methane, Combustion and Flame 212 (2020) 142–155. doi:10.1016/j.combustflame.2019.10.014.

[48] C.-W. Zhou, Y. Li, U. Burke, C. Banyon, K. P. Somers, S. Ding, S. Khan, J. W. Hargis, T. Sikes, O. Mathieu, E. L. Petersen, M. AlAbbad, A. Farooq, Y. Pan, Y. Zhang, Z. Huang, J. Lopez, Z. Loparo, S. S. Vasu, H. J. Curran, An experimental and chemical kinetic modeling study of 1,3-butadiene combustion: Ignition delay time and laminar flame speed measurements, Combustion and Flame 197 (2018) 423–438. doi:10.1016/j.combustflame.2018.08.006.

[49] L. Zhu, S. Panigrahy, S. N. Elliott, S. J. Klippenstein, M. Baigmohammadi, A. A. E. S. Mohamed, J. W. Hargis, S. Alturaifi, O. Mathieu, E. L. Petersen, K. A. Heufer, A. Ramalingam, Z. Wang, H. J. Curran, A wide range experimental study and further development of a kinetic model describing propane oxidation, Combustion and Flame 248 (2023) 112562. doi:10.1016/J.COMBUSTFLAME.2022.112562.